

Received 7 May 2024, accepted 28 May 2024, date of publication 30 May 2024, date of current version 7 June 2024.

Digital Object Identifier 10.1109/ACCESS.2024.3407734

RESEARCH ARTICLE

A Data-Driven Trajectory Approach for Dynamic VAR Support in Renewable Rich Power Grid

ABDULRHMAN ALSHAREEF¹, (Member, IEEE),
RAKIBUZZAMAN SHAH^{1b,2,3}, (Senior Member, IEEE),
N. MITHULANANTHAN², (Senior Member, IEEE), UMER AKRAM⁴, (Member, IEEE),
AND SAEED ALZHRANI^{1b,5}, (Member, IEEE)

¹Department of Electrical Engineering, University of Jeddah, Jeddah 21959, Saudi Arabia

²School of Electrical Engineering and Computer Science, The University of Queensland, Saint Lucia, QLD 4072, Australia

³Centre for New Energy Transition Research (CfNETR), Federation University Australia, Mount Helen, VIC 3353, Australia

⁴DigSILENT Pacific, Sydney, NSW 2000, Australia

⁵Electrical Engineering Department, Faculty of Engineering, Al-Baha University, Al-Baha 65779, Saudi Arabia

Corresponding author: Rakibuzzaman Shah (rakibuzz@gmail.com)

This work was supported by the Research, Development, and Innovation Authority (RDIA)-Kingdom of Saudi Arabia under Grant 12993-UJ-2023-UJ-R-3-1-SE. The work of Abdulrhman Alshareef was supported by the University of Jeddah, Saudi Arabia, for sponsoring his postgraduate study at The University of Queensland, Australia, through the Saudi Cultural Bureau in Australia, from 2018 to 2022.

ABSTRACT Short-term voltage stability (STVS) of power grids could be jeopardized due to the nonlinear dynamic characteristics of loads such as induction motors (IMs) and the retirement of synchronous generators. Moreover, the appearance of inverter-based generators (IBGs) in the system would make the grids more susceptible to voltage instability. Hence, there is an indispensable need to identify adequate mitigation measures to deal with these enduring challenges. This paper proposes a driven-data trajectory approach to locate the dynamic VAR support (DVS) to maintain STVS in power grids with high penetration of IBGs. The proposed data-driven trajectory approach ranks the best locations for DVS by comparing grid responses of different possible DVS sites with respect to the desired reference response. The developed approach covers the full signature of grid dynamics in generation and load sides. For illustration, this approach is applied to the Reliability and Voltage Stability (RVS) test system designed for STVS analysis. Several scenarios are tested, including various IM penetrations and IBG integration, control and load compositions, to demonstrate the viability and robustness of the proposed approach. Moreover, the STVS performance of the system with the proposed algorithm is verified through the motor stalling scan. The comprehensive assessment shows that the system exhibits the best STVS performance with DVS placement using the proposed method.

INDEX TERMS Alignment factor, data-driven trajectory, dynamic signature, Euclidean inner product, load dynamics, motor stalling, PV generator, short-term voltage stability.

I. INTRODUCTION

The power system experiences the reduction of ancillary services such as reactive power support, frequency and voltage regulation as synchronous generators (SGs) are replaced by inverter-based generators (IBGs). In addition, the IBGs have a limited ability to be overloaded for a shorter period compared to the SGs. Furthermore, the load compositions are everchanging and getting complex, resulting in inaccurate

The associate editor coordinating the review of this manuscript and approving it for publication was Sarasij Das^{1b}.

load modelling and parameterization. These trends contribute to significant changes and challenges in controlling power systems. The stability of the systems is getting complex, with voltage stability becoming a concern for the system operators.

The term voltage stability articulates the ability of the grid to maintain acceptable voltages after being subjected to disturbances. It can be classified into two categories, e.g., long-term and short-term voltage stability (STVS) [1]. The time scale for the long-term voltage stability is in the range of minutes, whilst the time scale for the STVS ranges between 0-10 s. Therefore, the STVS is more related to the dynamics

of the system. Voltage instability incidents could be triggered by reactive power deficiency in the network with high renewable penetrations [2], [3], [4]. Moreover, the STVS is strongly related to the complex dynamics of the loads, such as the induction motor and non-linear behaviour of power electronic loads [1], [3]. The voltage drop caused by the faults leads to the deceleration of induction motors. Subsequently, when the disturbance is cleared, the voltage starts to recover, and the induction motors consume high reactive demand to restore their speed. This rapid progressive mechanism stresses the power system, threatens system stability and eventually leads to the so-called fault-induced delayed voltage recovery (FIDVR) phenomenon [5], [6]. It is accepted that the FIDVR is strongly affected by IMs, the proliferation of IBGs and the replacement of the synchronous generators by IBGs [3], [7]. Unlike synchronous generators, the IBGs cannot substantially contribute to the short-circuit current to support STVS during and after the disturbances [4]. Furthermore, the IBGs may disconnect under some circumstances during the disturbance. This would stress the system further and reduce the STVS margin of the system [8].

Several countermeasures are applied by utilities to prevent or alleviate instability and improve the STVS margin of the system. For example, protection schemes could be designed and implemented on the demand side to quickly disconnect IMs, mostly air-conditioner loads in the residential sector, prior to stalling [9]. Other solutions include reducing the fault-clearing time and performing load-shedding schemes [6]. However, the integration of centralized VAR sources is accepted by utilities as the most effective solution to resolve the STVS [10], [11]. Hence, the allocation of DVS in power systems has been considered one of the main research interests in the voltage stability area.

The DVS allocation to resolve FIDVR appears in several works. In [10], the DVS location is nominated based on the sensitivity of VAR injection at certain buses and overall post-fault voltages. Optimal power flow (OPF) analysis was utilized to select the best location for DVS. The dynamic VAR placement is mainly done using a steady-state analysis, i.e., the power flow solution is linearized around a certain operating point. Although the time-domain simulations are involved in DVS allocation, the methodology is based on voltage sensitivity with respect to VAR injection using a network linearization model. Another approach to DVS siting is utilizing optimization techniques such as linear programming (LP) algorithm, Genetic Algorithm (GA), and others to allocate DVS [11], [12]. Those “intelligent” methods improve elite solutions during the optimization process using human reasoning principles to overcome the non-linearity of the main problems. However, most optimization techniques use objective functions based on linearized operating conditions. Moreover, these optimization techniques sometimes do not guarantee global optimization and may be settled to a locally optimal solution. The linear sensitivity methods for reactive power injection are proposed in the literature for STVS

assessment and DVS placement. However, these methods only considered the steady-state analysis with a few contingency cases. Furthermore, the replacement of synchronous generators with large-scale renewables is not considered [13], [14]. Besides, the prior stated methods do not consider the complete dynamics of the system.

A few studies have considered short-term voltage stability indices such as the transient voltage stability severity index (TVSI) and trajectory violation index (TVI) for short-term voltage stability assessment and placement of dynamic VAR resources. However, TVSI suffers from voltage oscillation, while TVI is case-dependent. The voltage recovery index has been improved in [15] for short-term voltage assessment. This method used the probability density function as well as the self-impedance of the load buses for the short-term voltage stability assessment. Another strategy of DVS allocation is evaluating the grid responses with DVS at various locations [16]. The proposed methods do not consider the entire system dynamics, from the generator to the load side. The work in [17] used fuzzy logic and a data-driven method to develop a voltage stability index from the generator limit. Research has been made to use machine learning methods for short-term voltage stability assessment in real-time [18]. However, neither of these works is in the planning domain and is already considered adequate reactive power resources available in the power system for remedial action. Furthermore, a large number of renewable energy sources are also scattered in the distribution system (e.g., medium and low voltage distribution networks). Besides the growing use of IBGs, the integration of power electronic loads is also impacting the electricity demand. However, most load models used in STVS studies are still basic, yet to consider the distribution system IBGs and power electronic loads [19], [20].

Advancements in measuring and monitoring power systems, such as phasor measurement units (PMUs), have allowed for access to more data about the power system. This includes operational data, historical voltage, current, and angle data, external system information, and more [21]. Data-driven approaches in power systems can identify the system's dynamic characteristics without the need for an exact and accurate parametric model, which can be challenging to obtain. The widespread use of sensing and recording enables the use of both model and data-driven methods for stability studies in power systems [22], [23], [24]. Direct and indirect methods can be used for data-driven analysis and control design. The indirect method involves using historical data of the power system to identify the system model explicitly. However, finding the appropriate parametric model can be challenging due to the diverse and evolving components of modern power systems [23], [24]. The direct method involves using recorded or real-time power system information without explicitly modelling the parametric model to design controllers, analyze power system dynamic behaviours, and arrange corrective actions [23], [24]. In this work, we have

TABLE 1. Comparison of the proposed method with previous works.

Ref.	Generator & load dynamics	Distribution IBGs and power electronic loads	Elimination of oscillation	Composite stability
[10]-[12]	x	x	x	x
[13],[14]	x	x	x	x
[15] [*]	√	x	x	x
[17],[18] [*]	√	-	√	x
Proposed	√	√	√	√

^{*}Only generator dynamics or limit

used a combination of a model-based approach and a direct data-driven method.

To the best of the author's knowledge, there are currently limited research efforts that encompass the placement of dynamic voltage support (DVS) on multiple power system dynamics phenomena in a renewable energy-rich power system. Due to different and even opposite impacts of any new devices on individual stability aspects, there is clearly a need for combined stability assessment considering multiple stability aspects. The major differences between the current work and previous works/studies are summarized in Table 1.

The proposed work here overcomes the main drawbacks, such as avoiding the selection and tuning of solution parameters. This will be discussed later in the mathematical derivation. The proposed approach is a data-driven approach considering the entire voltage trajectory of a given power system involving all the dynamic interactions through time-domain simulations. It is labelled as data-driven because the DVS siting is based on the comparison grid performance against the different candidates of DVS sites concerning the reference or desired performance over several small-time steps. The DVS allocation is a long-term planning study resulting in a critical decision to invest in installing DVS. Thus, the computational time and number of scenarios are given lower priority in these studies, contrary to short-term operational studies (i.e., remedial action plans). The proposed methodology has three main stages, e.g., determining the desired or reference voltage responses, evaluating the grid performance with different DVS locations, and verifying the selected location's performance.

The main contributions of this paper can be summarized as follows:

- A simple data-driven systemwide alignment factor is proposed for voltage responses (Section III. A).
- Proposed a trajectory-based method for dynamic Var system placement in a renewable rich power system (Section III-B).
- Detection method for oscillatory voltage response using moving Standard Deviation (movSD) (Section III. A).
- A fundamental study of complex load models and distributed energy resources on short-term voltage stability with DVS placement using the proposed index (Section V-D).

TABLE 2. RVS test system (base case information).

Item	Value
Nominal frequency (Hz)	60
Number of buses	75
Number of lines	33
Number of transformers	56
Number of generators	32
Number of loads	17
Number of SVCs (original base case)	2
Generation (MW)	3200
Demand (MW)	3135

- Verification of DVS siting methodology and system performance by scanning the motor stalling (Section V).
- Assess the impact of DVS placement on multiple aspects of the power system dynamics (Section V-F).

The remainder of this paper is divided into the following sections. The system description is given in Section II. Section III describes the theoretical background including the derivation of the systemwide alignment factor. The systematic methodology for DVS allocation is given Section IV. Section V provides case studies to demonstrate the efficacy and the robustness of the proposed methodology. Discussion and conclusions are presented in Section VI.

II. MODELLING OVERVIEW

A. TEST SYSTEM

The Reliability and Voltage Stability (RVS) test system illustrated in Fig. 1 has been used for the study. This test system has initially been developed for reliability and voltage stability assessments [25], [26]. The summary of the RVS test system is given in Table 2. All generator dynamics are considered, including the exciter system (parameters of the exciter system are given in Appendix A). Governor and stabilizer are used for some generators. The loads are connected to 13.8 kV buses through two-winding step-down transformers. The load model of the original system has been modified to add the detailed dynamics of the load as well as the distribution system IBGs and power electronic loads. The RVS test system originally had two static VAR compensators (SVCs) located at bus 106 and 114 with -50/+100 and -50/+200 MVar, respectively.

B. LOAD MODELLING

Voltage dynamics in a system are closely related to the load dynamics [19], [20]. Therefore, the appropriate model of the load and parameters should be used for the study. This section briefly explains the static and dynamic models considered in this study. Firstly, an elliptical current-voltage characteristic is used to model the static portions of the loads [27], [28]. The static load model holds constant MVA as long as the load terminal voltage exceeds the predefined threshold value (a threshold value of 0.7 pu is considered in this work). The load MVA is modified based on predefined current-voltage

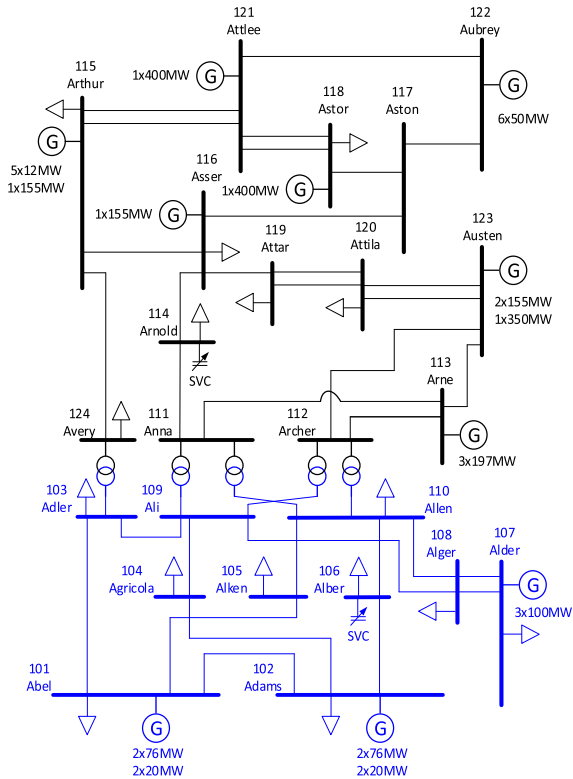


FIGURE 1. Single-line diagram of RVS test system [25], [26].

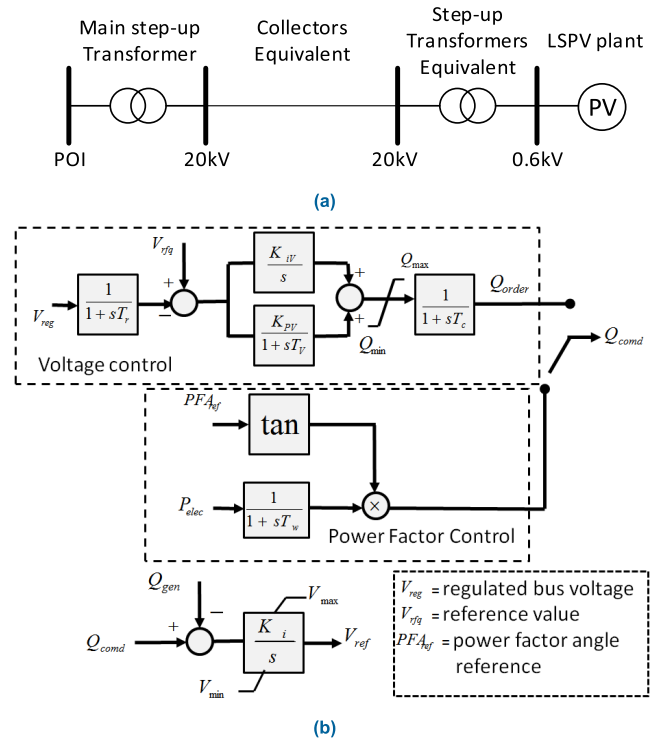


FIGURE 3. LSPV system model: (a) Single-machine equivalent model of PV plant [2]; (b) Reactive power control system [31].

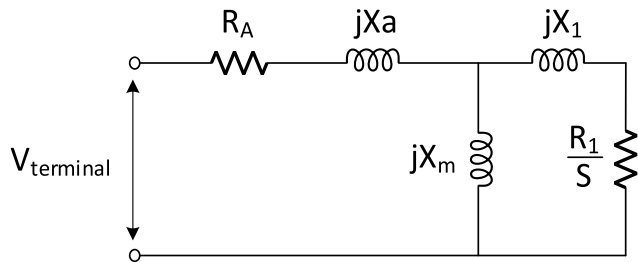


FIGURE 2. Induction motor equivalent circuit [29], [30].

characteristics [27]. Secondly, the dynamic load represents the rotational load, e.g., induction motors (IMs). As the load models and compositions play a vital role in the voltage stability analysis [29], [30], different penetration of IMs and their impacts are tested here. The IMs are modelled using the CIM5BL model. The CIM5BL model considers the entire transient behaviour of the motor. The two-axis model with rotor dynamics is considered in this study to represent the IM, as given in Fig. 2.

To evaluate the behaviour of the distribution system IBG and power electronic loads, we utilized the WECC composite load model, as mentioned in [19]. This model includes static and dynamic loads, divided into four motor classes. The proportion of dynamic loads and other loads can be adjusted to suit any specific system or case. The parameters used in this study are obtained from the references provided in [20] and therein.

C. LARGE-SCALE PV SYSTEM

The widely used WECC generic model of large-scale PV (LSPV) for stability studies is used here [2]. AC sides of PV inverters within the plant are aggregated to a single PV generator at the low voltage bus, as shown in Fig. 3. The PV generator delivers power to the grid through the collector circuit and the main step-up transformer to the point of integration (POI). Furthermore, three dynamic modules are attached to the PV generator to reflect the control strategy of LSPV, e.g., Generator/Converter (REGC_A) module, Electrical Control (REEC_B) module, and Plant Control (REPC_A) module. According to the grid codes in various transmission system operators (TSOs), the LSPV system support the grid voltage by injecting and absorbing the reactive power at the POI. This support service from the LSPV can be achieved by operating the inverter of the LSPV system either in voltage, reactive power or power factor control mode, as depicted in Fig. 3 (b). For the base case study, we have considered the reactive power control mode operation. Plant Control (REPC_A) sets the reference for the individual inverter control. The figure clearly shows that the voltage controller's meter device is modelled using a first-order function with time delay (T_r). In addition, a washout filter and lag time constant are used, as suggested in [31].

The VAR contribution of the LSPV system depends on the maximum converter current limit, which is normally 1.5 times the rated current during the sub-transient and transient timeframe. Different current limits (d and q -axis limits)

can be used for the converter-based generator. We have used the fixed current limit for this study with active current priority. The priority of active and reactive current inverter-based generator selection depends on transmission system operators' grid code requirements. EirGrid and Danish Grid have recommended the active current priority of PV, whereas National Grid UK and Fingrid have recommended reactive current priority [32]. It should be noted that the inverter-based generator, like PV, cannot overload for a short period during the fault. Moreover, reactive current injection during the fault may ignite overvoltage and voltage oscillation [32]. Hence, several works have advocated for active current priority [6], equal priority [33], and optimal active and reactive current injection over-reactive current priority (i.e., zero active currents during the fault) [32]. Furthermore, the optimal active and reactive current injection performs better than the reactive current injection-based method, as reported in [6]. Hence, this paper considered the active current priority-based method, which ramps up and down the active current to accommodate the reactive current during the fault.

Appendix B lists the parameters of the LSPV system. For this analysis, it should be noted that the LSPV plants are operated at plant-level control mode.

D. STATCOM

The static synchronous compensator (STATCOM) is a widely used DVS in power systems for voltage regulation [34], [35]. It is capable of injecting reactive current with an appropriate angle concerning the voltage to control the reactive power of the system. The STATCOM used the PWM converter between the DC source and the AC grid side. It used a phase-locked loop (PLL) to synchronize with the grid. The converter of the STATCOM generates the AC voltage from the DC side voltage. This study considered the electromechanical dynamics of the system. Therefore, the switching behaviour of the converter is considered ideal. The converter can be modelled using the average model, as shown in Fig. 4. From the figure, it can be seen that the model includes two PI controllers (i.e., the built-in-current controller), which estimate modulation index from the *d*-axis and the *q*-axis reference current. From the figure, it is also evident that the reference space (i.e., \cos_{ref}, \sin_{ref}) is obtained from PLL. The control parameters of the STATCOM used in this paper are taken from [34] and [35].

III. MATHEMATICAL OVERVIEW

A. DERIVATION OF ALIGNMENT FACTOR

The voltage response of *i*th load bus with the fault at *j*th bus can be expressed as (1).

$$V_i^j = [\dots, v_i^j(t - \Delta t), v_i^j(t), v_i^j(t + \Delta t), \dots]_{1 \times n} \quad \forall i, j \tag{1}$$

In (1), *v*, Δt , and *n* represent the instantaneous voltage, time step for the time-domain simulation, and total number of time steps, respectively. The voltage in (1) represents the original

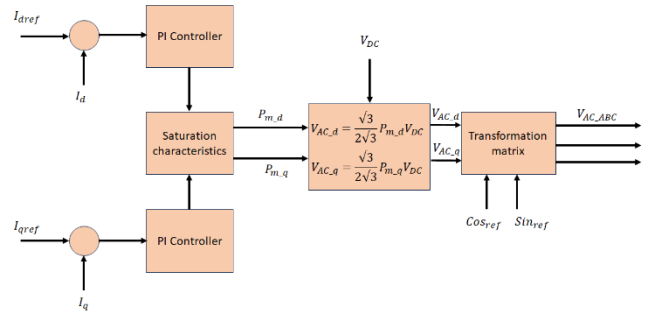


FIGURE 4. STATCOM with PI control block [35].

voltage response with all grid dynamics, regardless of IMs. Thus, V_i^j is considered to be the reference or desired voltage response of load buses. Practically, some of the transmission buses would be nominated to host centralized DVS based on several network planning factors, e.g., circuit breaker vacancy, and switchgear expansion feasibility. Therefore, let us assume that the number of candidate buses is ℓ and the list of candidate buses as \mathcal{L} . Let bus α be considered as the location of DVS connection where $\alpha \in [\mathcal{L}]_{1 \times \ell}$. Hence, the voltage response of *i*th bus under a fault at bus *j* (when DVS is connected to bus α), can be expressed as in (2):

$$U_{i,\alpha}^j = [\dots, u_{i,\alpha}^j(t - \Delta t), u_{i,\alpha}^j(t), u_{i,\alpha}^j(t + \Delta t), \dots]_{1 \times n} \quad \forall i, j, \alpha \tag{2}$$

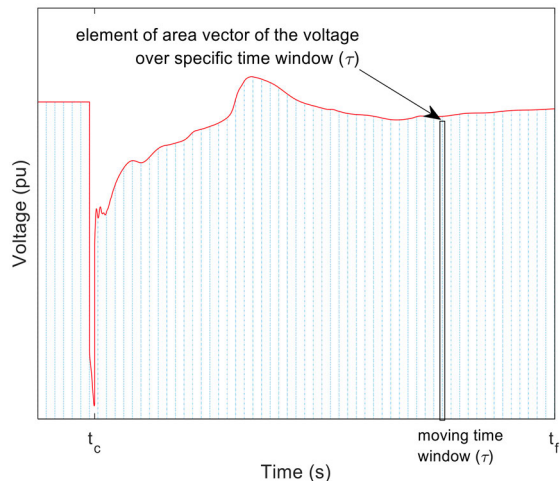
In (2), *u* is the instantaneous voltage at each time step. Let us define a sub-interval time sliding window as τ which contains a certain number of time steps (*k*). The sub-interval time τ is moving from clearing time *t_c* and exhaustively up to final observation time *t_f*. During the time-domain simulation, unwanted transients or spikes may appear in the voltage waveforms of V_i^j and $U_{i,\alpha}^j$. Hence, the voltage profiles V_i^j and $U_{i,\alpha}^j$ in (1) and (2) are converted to the form of the area vectors λ_i^j and $\lambda_{i,\alpha}^j$ to minimize the impact of these undesirable responses. The area vectors under the voltage responses V_i^j and $U_{i,\alpha}^j$ for each τ are given in (3) and (4), respectively.

$$\lambda_i^j = \int \bar{V}_i^j \quad \forall i, j \tag{3}$$

$$\lambda_{i,\alpha}^j = \int \bar{U}_{i,\alpha}^j \quad \forall i, j, \alpha \tag{4}$$

In (3) and (4), λ_i^j and $\lambda_{i,\alpha}^j$ are the area under \bar{V}_i^j and $\bar{U}_{i,\alpha}^j$. The voltages \bar{V}_i^j and $\bar{U}_{i,\alpha}^j$ are defined as the partial vectors from V_i^j and $U_{i,\alpha}^j$ with length *k* and sub-interval time τ . Therefore, Γ_i^j and $\Gamma_{i,\alpha}^j$ in (5) and (6) are defined as the area vectors with identical number of elements, $N = (t_f - t_c)/(\Delta t \times k)$. Fig. 5 shows a voltage response (*V*) with corresponding elements (λ). This represents the area under the partial vector (\bar{V}) from the voltage response (*V*) over the sub-interval time τ .

$$\Gamma_i^j = [\lambda_i^j]_{1 \times N} \tag{5}$$


FIGURE 5. Voltage response and area vector.

$$\Gamma_{i,\alpha}^j = [\lambda_{i,\alpha}^j]_{1 \times N} \quad (6)$$

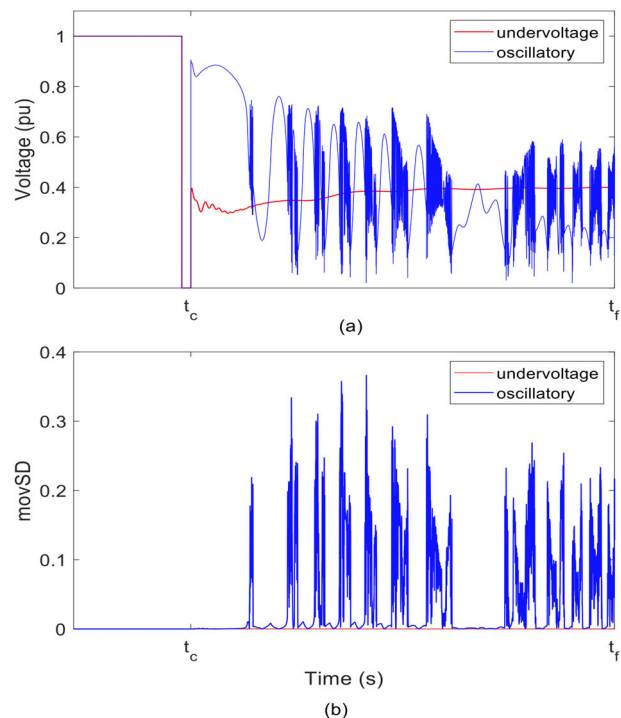
For power system planning studies, generally, there would be several scenarios to be evaluated and analyzed. However, it is not practical to plot and inspect all the cases. Moreover, the oscillations in different power system quantities could occur under disturbances due to non-linear interaction and system dynamic characteristics [30], [36]. The proposed method for determining the siting of the DVS involves the collection of data from PMU. The simulation estimates voltage, voltage angle, current, and current angle. The analysis included 75 different locations, each with different types of faults and fault resistance ranging from 0 to 48 ohms. In each fault scenario, faults were cleared within 80-120 ms. The simulation generated a dataset for the study that included ten different types of fault cases applied periodically, in addition to a no-fault scenario.

Furthermore, it is essential to differentiate the oscillatory voltage waveforms under the voltage instability events. Hence, the oscillation detection is performed using (7) and (8) by monitoring the sliding window standard deviation or the moving Standard Deviation (movSD) with the length k over sub-interval time τ [37].

$$\Psi_{i,\alpha}^j = \sqrt{\frac{1}{k-1} \sum_{\gamma=1}^k |\bar{U}_{i,\alpha}^j(\gamma) - \mu_{i,\alpha}^j|^2} \quad \forall i, j, \alpha \quad (7)$$

$$\mu_{i,\alpha}^j = \frac{1}{k} \sum_{l=1}^k \bar{U}_{i,\alpha}^j(l) \quad \forall i, j, \alpha \quad (8)$$

In (7) and (8), $\Psi_{i,\alpha}^j$, and $\mu_{i,\alpha}^j$ are movSD vector of $U_{i,\alpha}^j$, and mean of $\bar{U}_{i,\alpha}^j$, respectively. Fig. 6 (a) shows two undervoltage and oscillatory waveforms, and the corresponding movSD is depicted in Fig. 6 (b). The oscillation detection will be incorporated into this analysis through a decision variable $\xi_{i,\alpha}^j$, as given in (9). This decision variable would be equal to '1' when the non-zero elements in the movSD vector $\Psi_{i,\alpha}^j$ are less than the threshold percentage (ε). Otherwise, it would be equal to '0'. The threshold percentage (ε) is a user pre-defined


FIGURE 6. Oscillation detection for undervoltage and oscillatory voltage waveforms: (a) Voltage profile; (b) Corresponding movSD.

value selected to tolerate some natural oscillations after the fault clearance. In this analysis, a threshold percentage (ε) of 10% is considered.

$$\xi_{i,\alpha}^j = \mathbf{1}_{\{\Psi_{i,\alpha}^j < \varepsilon\}} \quad \forall i, j, \alpha \quad (9)$$

The optimal siting of DVS location can be determined using the area vectors Γ_i^j and $\Gamma_{i,\alpha}^j$ as given in (10) and (11).

$$\rho_{i,\alpha}^j = \frac{\Gamma_i^j \circ \Gamma_{i,\alpha}^j}{|\Gamma_i^j|^2} \xi_{i,\alpha}^j \quad \forall i, j, \alpha \quad (10)$$

$$K_\alpha = \frac{1}{n_{bus} \times F} \sum_{i=1}^{n_{bus}} \sum_{j=1}^F \rho_{i,\alpha}^j \quad \forall i, j, \alpha \quad (11)$$

In (10) and (11),

$\rho_{i,\alpha}^j$ is the alignment factor between V_i^j and $U_{i,\alpha}^j$ when DVS connected to bus α ;

K_α is the systemwide alignment factor between V ; and U vectors with the DVS connected to bus α ;

F is the number of fault locations;

The bus with the highest alignment factor (K_α) is the best location for DVS. The alignment factor K_α conceptually expresses the matching between the obtained responses and desired voltages over the similar time span. Alignment factor K_α is established mathematically based on the Euclidean Inner Product. Euclidean Inner Product is the generalization of the dot product. Principally, the Euclidean Inner Product of two vectors in R^2 or in the *Euclidean plane* is a scalar obtained by summing the multiplication of corresponding components

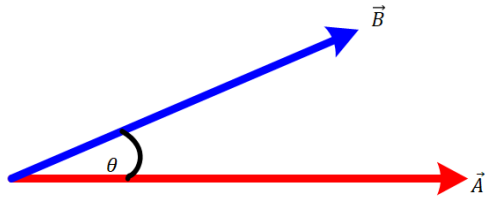


FIGURE 7. Vector \vec{A} and \vec{B} .

of two vectors [38]. Let us consider \vec{A} , \vec{B} , and \vec{C} as real space vectors. The inner product axioms of real vector space are listed in (12) to (16) [39], [40].

$$\langle \vec{A}, \vec{A} \rangle \geq 0 \tag{12}$$

$$\text{if } \langle \vec{A}, \vec{A} \rangle = 0 \text{ if and only if } \vec{A} = 0 \tag{13}$$

$$\text{if } \langle \vec{A} + \vec{B}, \vec{C} \rangle = \langle \vec{A}, \vec{C} \rangle + \langle \vec{B}, \vec{C} \rangle \tag{14}$$

$$\langle \alpha \vec{A}, \vec{B} \rangle = \alpha \langle \vec{A}, \vec{B} \rangle \text{ where } \alpha \text{ is a scalar} \tag{15}$$

$$\langle \vec{A}, \vec{B} \rangle = \langle \vec{B}, \vec{A} \rangle \tag{16}$$

The properties listed in (12) to (16) are satisfied when the magnitudes of voltages at each time step are real space vectors. This grounds the suitability of the inner product on voltage vectors. The researchers treat voltage waveforms from different valid perspectives. For instance, applying an entropy-based metric via the probability distribution function of the voltage waveforms based on signal processing and information theory [2], [16], [41]. The Entropy-based metric approach overcame several limitations of the classical methods of voltage response evaluation such as slope-based methods and integral error-based methods [2], [16], [41]. However, some solution parameters need to be assumed and tuned in an entropy-based metric approach to complete waveform evaluation. Here, with the vector space inner product concept, it is simply the sum of multiplications of corresponding voltage magnitudes at each time step and it yields a meaningful representative description of voltage response. To demonstrate the mathematical insight of the proposed alignment factor, let us unwrap the inner product to its origin, i.e., the dot product. In Fig. 7, \vec{A} and \vec{B} are the two real vectors in the plane. The projection of \vec{B} on \vec{A} is given in (17), which reflects the alignment between the two vectors. Furthermore, the alignment in (17) can be normalized based on the reference vector \vec{A} as expressed in (18).

$$|\vec{B}| \cos(\theta) = \frac{\vec{A} \cdot \vec{B}}{|\vec{A}|} \tag{17}$$

$$\text{alignment between } \vec{A} \text{ and } \vec{B} = \frac{\vec{A} \cdot \vec{B}}{|\vec{A}|^2} \tag{18}$$

B. MOTIVATING ILLUSTRATION

Samples of possible voltage waveforms are presented to provide an initial illustration of the proposed alignment factor (K_α). Fig. 8 depicts the different possible voltage waveforms that can be generated from time-domain simulations. The

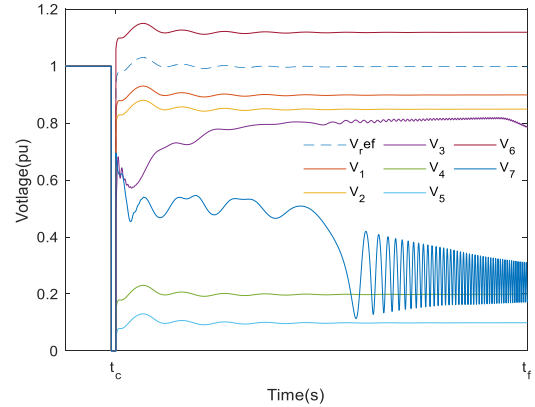


FIGURE 8. Various voltage profiles.

TABLE 3. Alignment factors for voltage given in Fig. 8.

	V_1	V_2	V_3	V_4	V_5	V_6	V_7
K_α	0.9101	0.8651	0.7987	0.2807	0.1908	1.1079	0

blue-dashed waveform is assumed as the reference or desired voltage response. Table 3 shows the alignment factor for each voltage response illustrated in Fig. 8. It is distinctly illustrated in Table 3 that the alignment factor (K_α) of voltage profiles reflects the alignment between the voltage responses and the reference voltage (V_{ref}). Furthermore, the oscillatory voltage of (V_7) could successfully be detected through the decision variable in alignment factor expression.

C. MOTOR STALLING SCAN

The motor stalling phenomenon and its related consequences, such as fault-induced delayed voltage recovery (FIDVR), are well addressed and established in the literature [16], [42]. The eventuality of motor stalling and FIDVR triggers when a sudden voltage drop occurs due to a fault in the load side with the high penetrations of IMs. Immediately, the IMs start decelerating because of voltage drops at their terminals. Once the fault is eliminated, terminal voltages of IMs begin to recover, and the IMs start to accelerate again, eventually leading to high instantaneous reactive power demand. In extreme cases, the power system may experience load shedding, cascaded tripping, or blackouts due to insufficient reactive power reserve. By monitoring the motor speed, the IM stalling can be identified. Based on this, a motor stalling scan algorithm is developed by monitoring motor speed variation. The motor stalling pseudo codes are given in Table 4.

IV. DVS SITING FRAMEWORK

Fig. 9 presents the framework to rank the DVS sites to alleviate STVS issues triggered by the higher penetration of LSPVs and IMs. The framework comprises three main steps. Step-I is a preliminary step to identify the study scenarios, including the disturbance selection, preparing the desired reference voltage via time-domain simulation, and identifying the DVS sites. In this analysis, all 230 and 138 kV buses are nominated

TABLE 4. Motor stalling scan pseudo code.

Steps
1: Solve load flow of the network;
2: Initialize network dynamic models;
3: Record initial IMs Δ speed;
3: Apply disturbances (3ph fault);
4: Clear fault;
5: Run simulation to final observation time (t_f);
6: Record final IMs Δ speed;
7: Compare Δ speeds in steps 3 & 6 to identify stalled IMs;
8: Identify the motor stalling spots;

for DVS installation except buses 106 and 114 (which initially hosted DVS). Benchmarking the grid dynamic signature has been conducted to prepare the desired reference voltage. Each bus has different reference voltage responses as the grid dynamic signatures vary with disturbances. Based on different disturbances on the grid, the alignment factor will evaluate reference and response voltage profiles. Step II is the core process of the DVS siting framework. Here, identified disturbances and candidates of DVS sites from Step-I are passed to the PSS@E platform to run the series of time-domain simulations. The time step for the time-domain simulation should be similar to the previous step to keep the vector length of the voltage waveforms equal. The next task in Step II is to estimate the alignment factor while considering various disturbances, DVS location, and operating conditions. The outcome of this task is a single number, i.e., the alignment factor for each DVS site corresponding to desired references. The selection of the best location for DVS depends on the alignment factor. The site with the highest alignment factor is the best location for DVS installation. Step III is conducted to confirm the STVS improvement after installing DVS at the selected site, as outlined in Step II. The number of motor stalling is used here as the grid performance indicator.

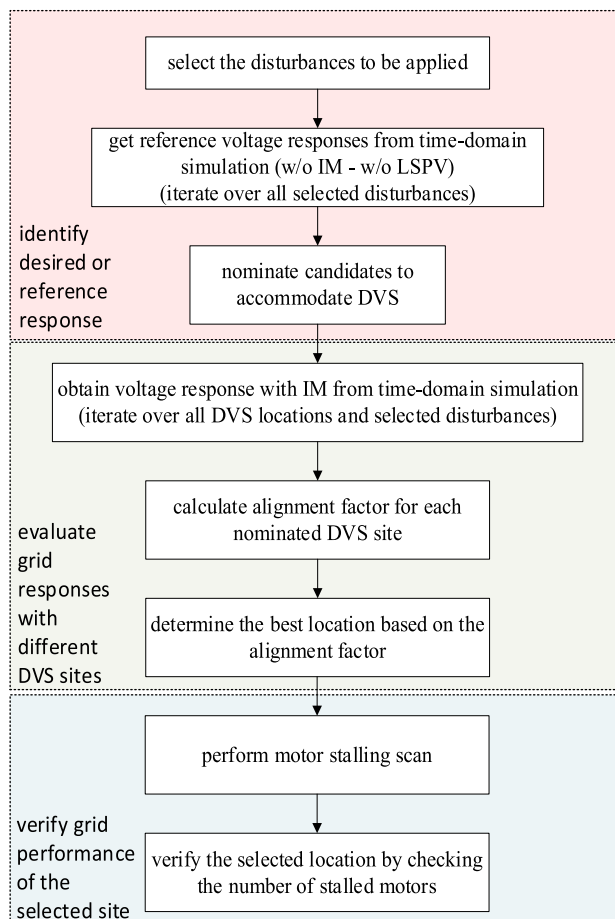
V. NUMERICAL EXPERIMENTS

This section demonstrates the application of the proposed DVS placement framework. A total of 22 DVS sites, 20 fault locations, and 17 load bus voltages are considered in the analysis to estimate the systemwide alignment factor. Different scenarios are tested and discussed in the sequel to validate the viability of the proposed DVS siting framework. We have used the following four cases to assess the efficacy of the proposed method.

- **Case A:** System with conventional generators.
- **Case B:** Uniform penetration of LSPVs.
- **Case C:** Replacement of bulk generator with LSPV plant.
- **Case D:** Composite load model with IBGs.

A. CASE STUDY A: SYSTEM WITH CONVENTIONAL GENERATORS

A total of 440 scenarios are simulated. Subsequently, each DVS site's alignment factor is computed to allocate DVS to

**FIGURE 9. Framework of the proposed DVS allocation.**

improve systemwide STVS performance. A motor stalling scan is also performed to ensure the proposed methodology's effectiveness. The motor stalling scan counts the number of stalled motors for each DVS site. Figs. 9 depict systemwide alignment factors ($K\alpha$) and the number of stalled IMs for different DVS locations for various IM penetrations.

Fig. 10 (a) shows that bus 109 has the highest alignment factor and, therefore, is the best location to install DVS. This outcome is verified as the number of stalled motors reduced from initial 33 motor stalling cases to non-stalled motors after adding DVS at bus 109 (see Fig. 10 (b)).

The alignment factors for higher IM penetrations, i.e., 25% and 30%, also exhibit a similar trend, as depicted in Fig 9 (a). The results evince that the sites with high alignment factors experience the lowest number of STVS issues, i.e., fewer stalled motors. Contrariwise, bus 122 in Fig.10 (a) shows the smallest alignment factor and higher number of stalled motors for all IM penetration levels. Figs. 11 (a) to (d) show grid responses with DVS installed in different sites. Precisely, Figs. 11 (a) and (b) represent the two best sites for DVS installation. Oppositely, Figs. 11 (c) and (d) show grid responses for the two worst sites for DVS installation, i.e., the lowest alignment factor. From the figures, it is evident that

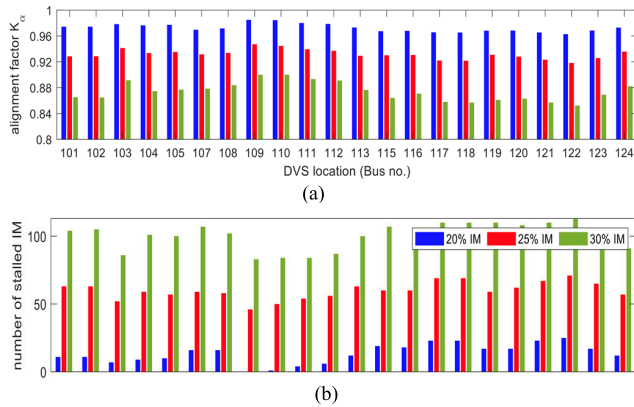


FIGURE 10. Placement of DVS for Case A: (a) Alignment factor; (b) Number of stalled motors.

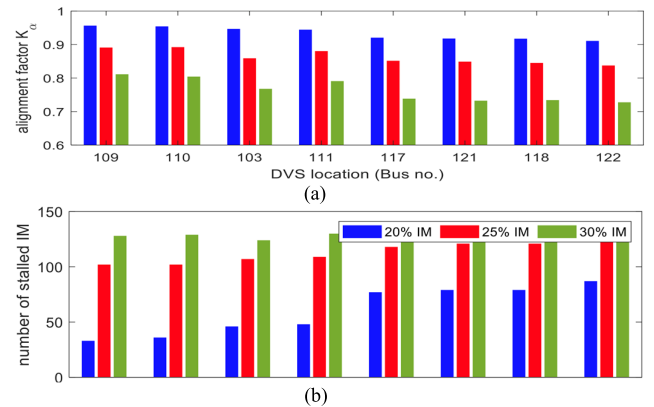


FIGURE 12. Placement of DVS for Case B: (a) Alignment factor; (b) Number of stalled motors.

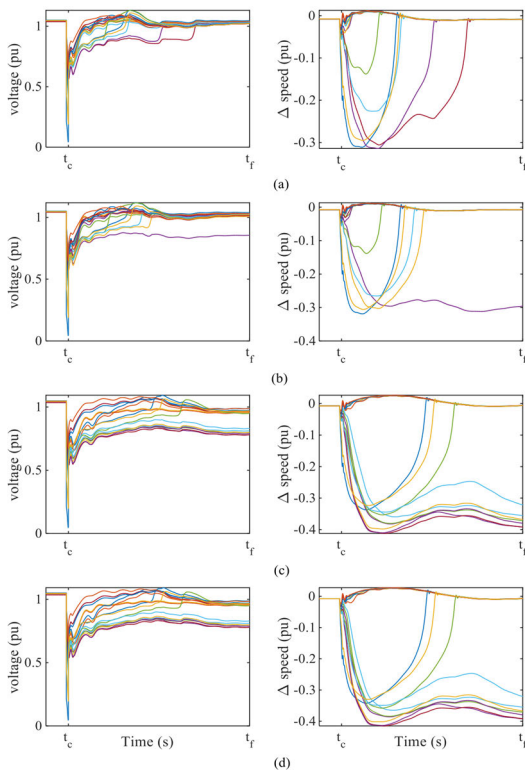


FIGURE 11. Voltage and IM speed responses (IM 20%): (a) DVS @ bus 109; (b) DVS @ bus 110; (c) DVS @ bus 121; (d) DVS @ bus 122.

the system experiences higher STVS margins when the DVSs are placed on buses with higher alignment factors. From the results, it is evident that the system would experience lower STVS margins when the DVSs are connected to buses 121 and 122 (the worst location for DVS identified by the proposed method).

B. CASE STUDY B: UNIFORM PENETRATION OF LSPVS

In this scenario, one generator at each plant of the RVS system is replaced by the LSPV except for plants 118, 121, and 122 (because they are the nuclear and hydro plants).

The integration level of LSPV would be around 15% of the generation mix. Figs. 12 depict the systemwide alignment factors ($K\alpha$) and the number of stalled IMs for selected DVS locations considering three different IM penetrations.

The trend formed in Fig. 12 (a) is also consistent, similar to Fig. 10 (a); the higher alignment factor means a lower number of stalled motors and a better STVS margin. Similar trends could be observed for all levels of IM penetration. The voltage profiles and changes in motor speed for all load buses for uniform LSPV with 20% IM penetration are given in Figs. 13 (a) and (d). Figs. 13 (a)-(b) show the grid responses with DVS for the two best sites. Also, two worst cases are given in Figs. 13 (c) and (d).

The comparison between Fig. 10 and Fig. 12 outlines the impact of uniform LSPVs on STVS margin. For illustration, the alignment factor with conventional generators (SGs) is higher than the case when LSPVs replaced some SGs. Contrary to this, the number of stalled motors with SGs is lower than the case with uniform penetration of LSPV. Comparing Fig. 11 and Fig. 13, it is evident that the LSPV integration is clearly jeopardizing STVS performance, as noticed in the voltage recovery and motor speeds. The lower STVS margin with the LSPV plants is expected even with dynamic support services provided by LSPVs. This is observed due to the limited reactive current capability of LSPV than the SGs. Although the motor stalling events are observed, the integration of DVS at bus 109 has reduced the number of motor stalling. Nonetheless, the remaining STVS issues would be resolved after adding a second DVS at bus 110 (which has the second-highest alignment factor).

C. CASE STUDY C: REPLACEMENT OF BULK GENERATOR WITH LSPV PLANT

In this case, a conventional bulk generator is replaced by the LSPV plant. To test this scenario, a bulk generator at 113 with the capacity of 487 MW is substituted with the LSPV plant. This bulk replacement brings the LSPV penetration level to around 15%. Based on the proposed approach of DVS siting, DVS at bus 108 shows the best grid performance, which

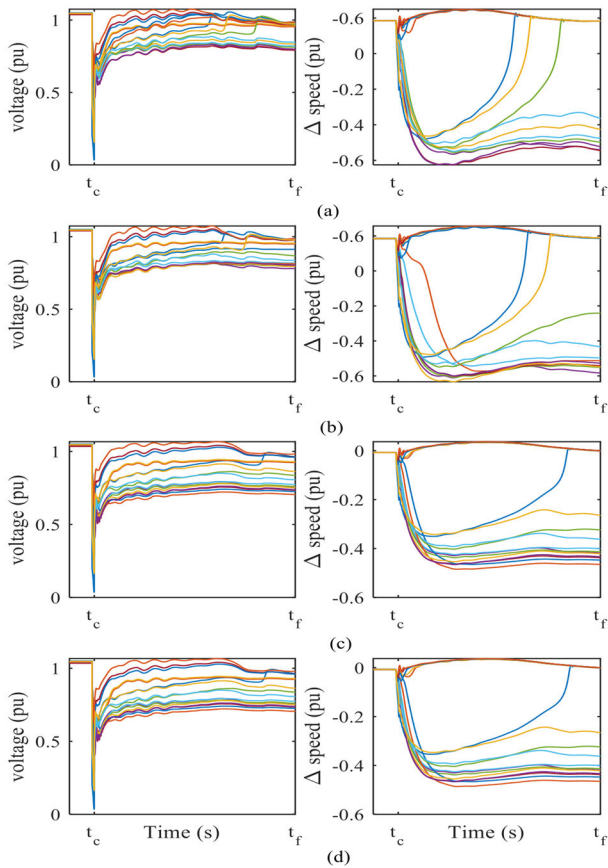


FIGURE 13. Voltage and IM speed responses (uniform LSPV plants & IM 20%): (a) DVS @ bus 109; (b) DVS @ bus 110; (c) DVS @ bus 121; (d) DVS @ bus 122.

has been consistently verified with the number of stalled motors. Similar to Figs. 10 and 12, Fig. 14 shows alignment factors and the number of stalled motors for DVS sites with various IM penetration levels. The trend comprised here is also consistent. A higher alignment factor means lower STVS issues and better possible STVS performance. Similar trends are observed for all levels of IM penetration. The voltage profiles and changes in motor speed for all load buses with LSPV are given in Fig. 15. The extreme case is explained under this scenario. The grid experiences severe instability cases, grid collapse and loss of synchronization. The bulk LSPV integration is clearly jeopardizing STVS performance, as noticed in the voltage recovery and motor speeds shown in Fig. 15. This is a foreseeable situation to see more instability cases in bulk SGs retirement compared to the uniform pattern of LSPV plant integration. This happened due to the integration of the LSPV in the significantly weak area of the grid strength. Therefore, further endangering the grid strength. However, installing more DVSs according to the best DVS sites obtained based on alignment factors will maintain grid stability, as shown in Fig. 16.

D. CASE STUDY D: COMPOSITE LOAD MODEL WITH IBGS

This section assesses the STVS performance of the system with composite load and the distribution system IBGs. Fig. 17

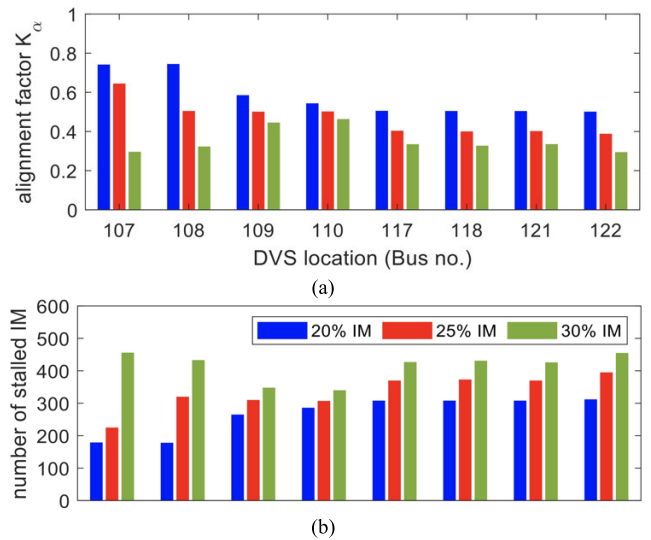


FIGURE 14. Placement of DVS for Case C: (a) Alignment factor; (b) Number of stalled motors.

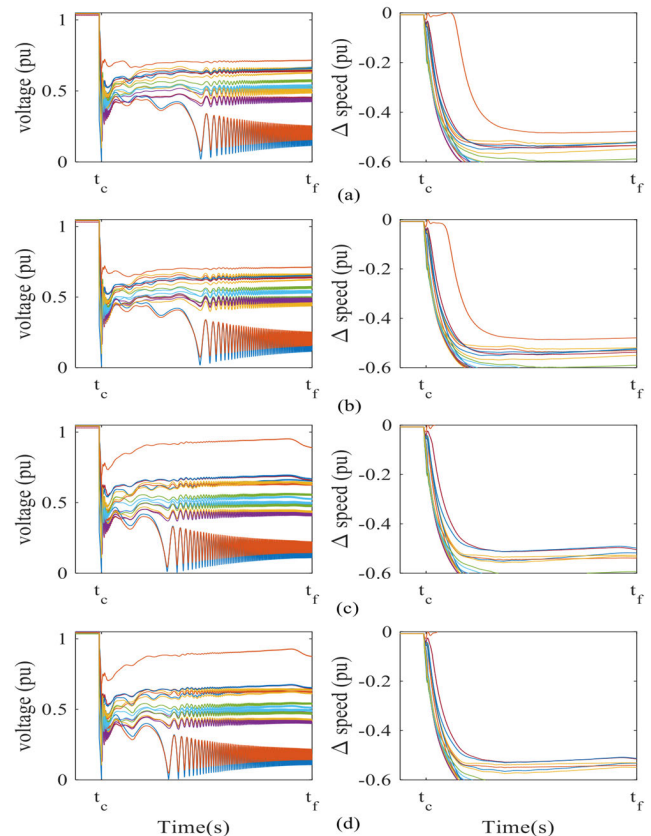


FIGURE 15. Voltage and IM speed responses (bulk LSPV plant penetration & IM 20%): (a) DVS @ bus 109; (b) DVS @ bus 110; (c) DVS @ bus 121; (d) DVS @ bus 122.

shows the STVS performance with DVS at bus 109 and 122. From the results in Fig. 17, it is evident that the hosting of the IBGs can be increased with the DVS placement at the best site determined by the proposed method. Fig. 18

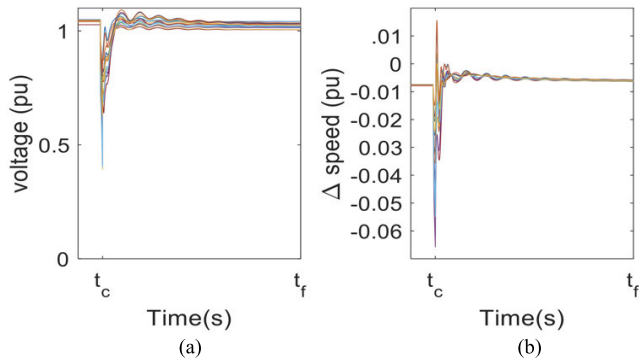


FIGURE 16. Voltage and IM speed responses (bulk LSPV plant penetration & IM 20%): (a) Voltage responses for DVS @ bus 108,109,111, and 112; (b) Speed deviation of the IMs.

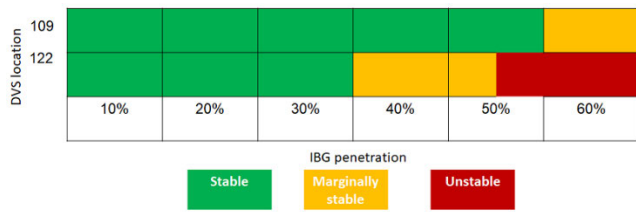


FIGURE 17. Correlation heatmaps of various IBGs and DVS locations.

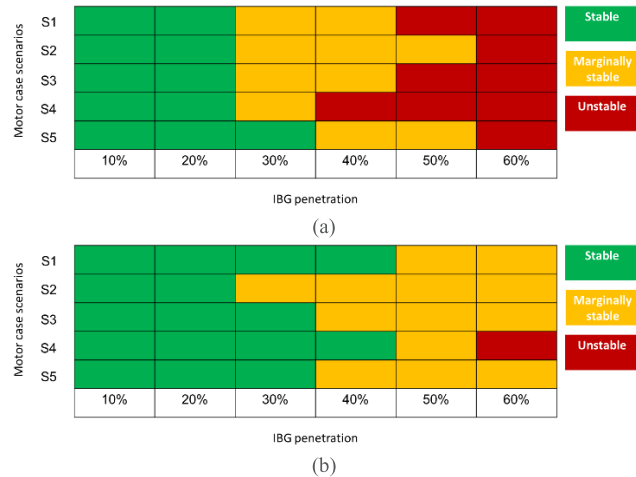


FIGURE 18. Correlation heatmaps of various IBGs and load scenarios: (a) Without DVS; (b) With DVS.

compares the STVS performance for the different load compositions. The load model composition scenarios are given in Table 5. The load is modelled using the model presented in [43]. It is important to note that the IBGs are replacing the SGs in the system without complementing them. This can lead to voltage stability constraints in the absence of effective DVS placement. However, placing DVS at optimal locations can significantly reduce concerns about voltage stability.

E. COMPARATIVE STUDY

The proposed alignment factor-based method for DVS placement is compared here with the trajectory-based method

TABLE 5. Load composition scenarios.

Scenarios	Description	Share of motor
S1	More A - type	0.3/0.1/0.1/0.1
S2	More B - type	0.1/0.3/0.1/0.1
S3	More C - type	0.1/0.1/0.3/0.1
S4	More D - type	0.1/0.1/0.1/0.3
S5	Equal share	0.15/0.15/0.15/0.15

TABLE 6. Comparative study.

LSPV integration	IMs (%)	Method	DVS location	Number of stalled motors
Uniform LSPV	20	Proposed	109	30
		Trajectory [44]	112	52
		Sensitivity [14], [45]	113	55
	25	Proposed	109	100
		Trajectory [44]	112	143
		Sensitivity [14], [45]	113	144
	30	Proposed	109	133
		Trajectory [44]	112	178
		Sensitivity [14], [45]	113	180
Replace bulk generation by LSPV	20	Proposed	108	150
		Trajectory [44]	115	183
		Sensitivity [14], [45]	114	183
	25	Proposed	108	200
		Trajectory [44]	115	234
		Sensitivity [14], [45]	114	237
	30	Proposed	108	250
		Trajectory [44]	115	287
		Sensitivity [14], [45]	114	287

in [44] and the sensitivity-based method in [45]. The trajectory sensitivity of DVS siting is obtained by observing the sensitivity of VAR injection on the system voltage profile at different time instants during the simulation in the time horizon. The sensitivity-based method used the steady-state analysis-based index, as stated in [44]. The comparative results for various penetrations of IMs and LSPVs are given in Table 6. From the results given in Table 6, it is evident that the proposed method outperformed other commonly reported methods in the literature. Therefore, the proposed alignment factor approach is more suitable for DVS siting.

The robustness of the proposed DVS placement method is tested in this section and reported. Different integrations of LSPV and the reactive power and voltage control of LSPV are used for this assessment. This analysis has been done for 25% of the penetrations of IM. The assessment results are given in Table 7. From the results given in Table 7, it is evident that the proposed method invariably identifies the best location for DVS placement to improve the STVS margin of the system.

The proposed placement method’s robustness has been tested for the LSPV’s reactive current priority. The results of the assessment using the PV system’s Q-V control are

TABLE 7. Robustness of the method.

PV integration	PV system control	VAR placement method	DVS bus	Number of stalled motors
Uniform integration	Voltage control	Proposed	109	30
		Trajectory [44]	112	52
		Sensitivity [14], [45]	113	55
	Q-V control	Proposed	109	15
		Trajectory [44]	112	32
		Sensitivity [14], [45]	113	35
	Power factor	Proposed	109	42
		Trajectory [44]	112	62
		Sensitivity [14], [45]	113	65
Bulk generator replaced by PV	Voltage control	Proposed	108	150
		Trajectory [44]	115	183
		Sensitivity [14], [45]	114	183
	Q-V control	Proposed	108	95
		Trajectory [44]	115	143
		Sensitivity [14], [45]	114	147
	Power factor	Proposed	108	162
		Trajectory [44]	115	187
		Sensitivity [14], [45]	114	188

TABLE 8. Robustness of the proposed method with respect to current limits.

PV integration	PV system current limits	DVS bus	Number of stalled motors
Uniform integration	Active current priority	109	15
	Reactive current priority	109	14
Bulk generator replaced by PV	Active current priority	108	95
	Reactive current priority	108	93

presented in Table 8. According to the table, the placement method suggested in this paper is not influenced by the LSPV’s various current limits, which proves the proposed method’s practicality.

Furthermore, we have also examined the computation time of the proposed method. The computational time for each single time-domain simulation scenario is 37 seconds using a PC with i7-8700@ 3.20GHz Intel Core (TM) CPU with 16 GB RAM.

F. COMPOSITE STABILITY ASSESSMENT

It is vital to execute a rigid assessment of any new devices on the interdependence of power system dynamics [46]. The dynamic VAR devices could affect other stability issues in power systems other than STVS. Therefore, the impact of the placement of DVS on combined or composite stability (CSI) is used in this work to evaluate the combined system stability from two aspects, i.e., small-signal stability and large-disturbance rotor angle stability. At first, the individual

DVS location	IBGs penetration			
	15%	30%	45%	60%
109	0.91	0.86	0.82	0.78
110	0.87	0.81	0.77	0.73
122	0.76	0.73	0.68	0.63

FIGURE 19. CSI of the system for IBG penetrations and DVS locations.

stability indices are explained before presenting the normalized combined stability index.

The small-signal stability or small-disturbance stability is assessed here by the damping of the complex conjugate eigenvalues of the critical electromechanical (EM) mode. The well-known transient stability index (TSI) has been used for the large-disturbance rotor angle stability assessment. The TSI can be expressed as in (19) [47].

$$TSI = \frac{\delta_{limit} - \delta_{max}}{\delta_{limit} + \delta_{max}} \times 100 \tag{19}$$

In (19), δ_{limit} is the maximum rotor angle separation (i.e., 360^0) and δ_{max} is the maximum rotor angle deviation between two generators. TSI can vary between 0 to 100, where 100 means the more stable system. The Negative value of TSI indicates the large deviation of rotor angle leading to the loss of synchronization, i.e., unstable system, TSI value 0 means the violation of stability. Since the ranges of the individual index are different, therefore, we need to normalized the indices to develop the composite index. The normalization of the stability index corresponding to the largest distance can be expressed as in (20) and (21) [37].

$$\sigma_{nm} = \begin{cases} \frac{\sigma_{limit} - \sigma}{\sigma_{ref}}, & \sigma < 0 \\ 0, & \sigma \gg 0 \end{cases} \tag{20}$$

$$TSI = \begin{cases} \frac{TSI - TSI_{limit}}{TSI_{ref}}, & TSI > 0 \\ 0, & TSI < 0 \end{cases} \tag{21}$$

In (20) and (21), σ_{limit} and TSI_{limit} represent the limit of the small-disturbance stability and large-disturbance rotor angle stability, respectively, whilst σ_{ref} and TSI_{ref} represent the reference value for the stability distance.

Therefore, the composite stability index (CSI) can be expressed as in (22) [47].

$$\frac{1}{CSI} = 0.5 \times \left(\frac{1}{\sigma_{nm}} + \frac{1}{TSI_{nm}} \right) \tag{22}$$

In (22), 0.5 is used to consider both stability equally. The CSI varies between 0 to 1 for the stable system, where 1 means the most stable system.

Fig. 19 illustrates the CSI of the system with DVS in different locations (i.e., best, moderate and worst). We have used the composite load model and distributed IBGs for this analysis. Significant differences in CSI could be observed for DVS in different locations. The system experiences a high stability margin (i.e., high CSI) for the best DVS location, i.e.,

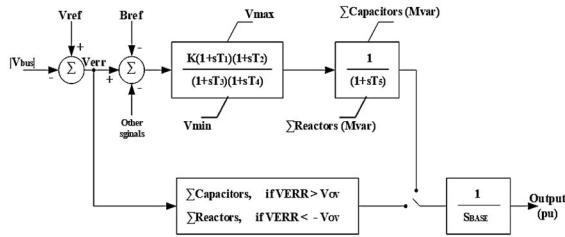


FIGURE 20. CSSCST model Block diagram as provided in PSS@E documents.

TABLE 9. CSSCST parameters.

Parameter	100/-50Mvar	200/-50Mvar
K (pu)	22500	37500
T_1 (s)	0	0
T_2 (s)	0	0
T_3 (s)	3.45	3.55
T_4 (s)	0	0
T_5 (s)	0.03	0.03
$VMAX$ (Mvar)	0	0
$VMIN$ (Mvar)	0	0
Vov - override voltage (pu)	0.5	0.5

TABLE 10. REGCA parameters.

Parameter	Value
T_g (s)	0.02
$Rpwr$ (pu/s)	10.00
$Brkpt$, LVPL voltage 2 (pu)	0.90
$Zerox$, LVPL voltage 1 (pu)	0.70
$Lvp11$, LVPL gain (pu)	1.00
$Volim$ (pu)	1.20
$Lvpnt1$ (pu)	0.05
$Lvpnt0$ (pu)	0.01
$Iolim$ (pu) (< 0)	-1.00
$Tfltr$ (s)	0.01
Khv (≥ 0 and < 1)	0.70
$Iqrmx$ (pu/s)	20.00
$Iqrmin$ (pu/s)	-20.00
$Accel$ (> 0 and ≤ 1)	0.70

bus 109. It is worth noting that there is no significant difference in CSI between bus 109 and 110. However, significant differences of CSI could be observed for the best and worst DVS location. It should be worth noting that the number in each cell represents the CSI of the system.

VI. CONCLUSION

This paper proposed a data-driven approach to identify the best location for Dynamic VAR Sources (DVS). A systemwide alignment factor is used to assess STVS performance for each candidate site and the ranking of the sites. The alignment factor treats the voltage waveform obtained from time-domain simulations as space vector with mathematical justifications. Hence, the space vector inner product theory is employed to match the grid response with the desired reference response. The derived data-driven trajectory alignment factor covers the full grid dynamic signature imposed from the generation

TABLE 11. REECB parameters.

Parameter	Value
$Vdip$ (pu)	0.90
Vup (pu)	1.10
Trv (s)	0.01
$dbd1$ (pu) (≤ 0)	-0.10
$dbd2$ (pu) (≥ 0)	0.10
Kqv (pu)	4.00
$Iqhl$ (pu)	1.30
$Iqll$ (pu)	-1.30
$Vref0$ (pu) (if 0, initialized by model)	0.00
Tp (s)	0.01
$QMax$ (pu)	0.40
$QMin$ (pu)	-0.40
$VMAX$ (pu)	1.10
$VMIN$ (pu)	0.90
Kqp (pu)	0.05
Kqi (pu)	0.10
Kvp (pu)	12.00
Kvi (pu)	300.0
Tiq (s)	0.01
$dPmax$ (pu/s) (> 0)	1.00
$dPmin$ (pu/s) (< 0)	-1.00
$PMAX$ (pu)	1.00
$PMIN$ (pu)	0.00
$Imax$ (pu)	1.00
$Tpord$ (s)	0.01

TABLE 12. REPCA parameters.

Parameter	Value
$Tfltr$ (s)	0.02
Kp (pu)	0.36
Ki (pu)	0.18
Tft (s)	0.00
Tfv (s)	0.10
$Vfrz$ (pu)	0.00
Rc (pu)	0.00
Xc (pu)	0.00
Kc (pu)	0.00
$emax$ (pu)	0.10
$emin$ (pu)	-0.10
$dbd1$	-0.01
$dbd2$	0.01
$Qmax$ (pu)	0.40
$Qmin$ (pu)	-0.40
Kpg (pu)	1.00
Kig (pu)	10.00
Tp (s)	0.02
$fdbd1$	0.00
$fdbd2$	0.00
$femax$ (pu)	999.00
$femin$ (pu)	-999.00
$Pmax$ (pu)	1.00
$Pmin$ (pu)	0.00
Tg (s)	0.10
Ddn (pu)	20.00
Dup (pu)	10.00

and demand sides. The site with the highest systemwide alignment factor has been considered as the best location.

Furthermore, the motor stalling scan is performed to verify the outcomes of the proposed siting framework. The efficacy of the proposed method is tested in the RVS system suitable for voltage stability studies, particularly in the planning stages. The system consistently experiences a better

stability margin when the DVSs are placed by the proposed method. Furthermore, it is evident that the proposed method is superior compared to the existing sensitivity-based methods. The proposed framework also provides a ranking list of the candidate sites if more DVSs are required to maintain grid stability. Furthermore, the alignment factor sheds light on the possibility of using it as a systemwide index for assessing STVS. Moreover, the derivation of the alignment factor reveals the possibility of developing an index to quantify the voltage recovery for an individual bus. Besides, this proposed method can also be extended to minimize or select the size of DVSs with the high penetrations of renewable generations.

APPENDICES

APPENDIX A

The CSSCST model block diagram is shown in Fig. 20. The model parameters are given in Table 9.

APPENDIX B

This appendix section lists the detailed parameters of LSPV and illustrated in Tables 10–12.

REFERENCES

- [1] S. Alzahrani, R. Shah, and N. Mithulananthan, "Examination of effective VAR with respect to dynamic voltage stability in renewable rich power grids," *IEEE Access*, vol. 9, pp. 75494–75508, 2021.
- [2] G. Lammert, D. Premm, L. D. P. Ospina, J. C. Boemer, M. Braun, and T. Van Cutsem, "Control of photovoltaic systems for enhanced short-term voltage stability and recovery," *IEEE Trans. Energy Convers.*, vol. 34, no. 1, pp. 243–254, Mar. 2019.
- [3] A. Alshareef, R. Shah, N. Mithulananthan, and S. Alzahrani, "A new global index for short term voltage stability assessment," *IEEE Access*, vol. 9, pp. 36114–36124, 2021.
- [4] D. Wu, G. Li, M. Javadi, A. M. Malysheff, M. Hong, and J. N. Jiang, "Assessing the impact of renewable energy integration on system strength using site-dependent short circuit ratio," *IEEE Trans. Sustain. Energy*, vol. 9, no. 3, pp. 1072–1080, Aug. 2018.
- [5] A. C. Sullberg, M. Wu, V. Vittal, B. Gong, and P. Augustin, "Examination of composite load and variable frequency drive air conditioning modeling on FIDVR," *IEEE Open Access J. Power Energy*, vol. 8, pp. 147–156, 2021.
- [6] R. K. Varma and S. Mohan, "Mitigation of fault induced delayed voltage recovery (FIDVR) by PV-STATCOM," *IEEE Trans. Power Syst.*, vol. 35, no. 6, pp. 4251–4262, Nov. 2020.
- [7] F. Milano, F. Dorfler, G. Hug, D. J. Hill, and G. Verbič, "Foundations and challenges of low-inertia systems (invited paper)," in *Proc. Power Syst. Comput. Conf. (PSCC)*, 2018, pp. 1–25.
- [8] K. W. Jones, "Impact of inverter-based generation on bulk power system dynamics and short-circuit performance," *IEEE Power Energy Soc.*, Jul. 2018.
- [9] Y. Zhang, Y. Xu, Z. Y. Dong, and P. Zhang, "Real-time assessment of fault-induced delayed voltage recovery: A probabilistic self-adaptive data-driven method," *IEEE Trans. Smart Grid*, vol. 10, no. 3, pp. 2485–2494, May 2019.
- [10] W. Huang, K. Sun, J. Qi, and Y. Xu, "A new approach to optimization of dynamic reactive power sources addressing FIDVR issues," in *Proc. IEEE Power Energy Soc. Gen. Meeting (PESGM)*, vol. 2014, pp. 1–5.
- [11] A. M. Tahboub, M. S. El Moursi, W. L. Woon, and J. L. Kirtley, "Multiobjective dynamic VAR planning strategy with different shunt compensation technologies," *IEEE Trans. Power Syst.*, vol. 33, no. 3, pp. 2429–2439, May 2018.
- [12] A. Tiwari and V. Ajjarapu, "Optimal allocation of dynamic VAR support using mixed integer dynamic optimization," *IEEE Trans. Power Syst.*, vol. 26, no. 1, pp. 305–314, Feb. 2011.
- [13] J. Qi, W. Hunag, K. Sun, and W. Kang, "Optimal placement of dynamic Var sources by using empirical controllability covariance," *IEEE Trans. Power Syst.*, vol. 32, no. 1, pp. 240–249, Jan. 2017.
- [14] S. Wildenhues, J. L. Rueda, and I. Erlich, "Optimal allocation and sizing of dynamic var sources using heuristic optimization," *IEEE Trans. Power Syst.*, vol. 30, no. 5, pp. 2538–2546, Sep. 2015.
- [15] S. E. Sadeghi and A. Akbari Foroud, "A general index for voltage stability assessment of power system," *Int. Trans. Electr. Energy Syst.*, vol. 31, no. 12, pp. 1–22, Dec. 2021.
- [16] S. Dasgupta, M. Paramasivam, U. Vaidya, and V. Ajjarapu, "Entropy-based metric for characterization of delayed voltage recovery," *IEEE Trans. Power Syst.*, vol. 30, no. 5, pp. 2460–2468, Sep. 2015.
- [17] S. Shazadeh, H. Golpira, and H. Bevrani, "An adaptive data-driven method based on fuzzy logic for determining power system voltage status," *J. Modern Power Syst. Clean Energy*, vol. 99, pp. 1–11, Dec. 2023.
- [18] K. D. Dharmapala and A. D. Rajapakse, "Automated data labelling for machine learning based short-term voltage stability classification," in *Proc. CIGRE Canada Conf. Expo.*, 2022.
- [19] A. Boričić, J. L. R. Torres, and M. Popov, "Fundamental study on the influence of dynamic load and distributed energy resources on power system short-term voltage stability," *Int. J. Electr. Power Energy Syst.*, vol. 131, Oct. 2021, Art. no. 107141.
- [20] Z. Lv, B. Wang, Q. Guo, and H. Sun, "Optimal grid support strategy with inverter interfaces distributed generators for smart-term voltage stability improvement," *IEEE Trans. Sustain. Energy*, vol. 99, pp. 1–13, 2023.
- [21] O. Bertozzi, H. R. Chamorro, E. O. Gomez-Diaz, M. S. Chong, and S. Ahmed, "Application of data-driven methods in power systems analysis and control," *IET Energy Syst. Integr.*, vol. 2023, pp. 1–26, Jan. 2023.
- [22] L. Fan, Z. Miao, S. Shah, P. Koralewicz, V. Gevorgian, and J. Fu, "Data-driven dynamic modeling in power systems: A fresh look on inverter-based resource modeling," *IEEE Power Energy Mag.*, vol. 20, no. 3, pp. 64–76, May 2022.
- [23] L. Zhu, W. Wen, J. Li, and Y. Hu, "Integrated data-driven power system transient stability monitoring and enhancement," *IEEE Trans. Power Syst.*, vol. 39, no. 1, pp. 1797–1809, Feb. 2024.
- [24] Q. Wang, F. Li, Y. Tang, and Y. Xu, "Integrating model-driven and data-driven methods for power system frequency stability assessment and control," *IEEE Trans. Power Syst.*, vol. 34, no. 6, pp. 4557–4568, Nov. 2019.
- [25] T. Van Cutsem, M. Glavic, W. Rosehart, C. Canizares, M. Kanatas, L. Lima, F. Milano, L. Papangelis, R. A. Ramos, J. A. d. Santos, B. Tamimi, G. Taranto, and C. Vournas, "Test systems for voltage stability studies," *IEEE Trans. Power Syst.*, vol. 35, no. 5, pp. 4078–4087, Sep. 2020.
- [26] *IEEE Power System Dynamic Performance Committee*. [Online]. Available: <https://site.ieee.org/pes-psdp/489-2/>
- [27] A. Adrees and J. Milanović, "Effect of load models on angular and frequency stability of low inertia power networks," *IET Gener., Transmiss. Distrib.*, vol. 13, no. 9, pp. 1520–1526, 2019.
- [28] *PSS/E Program Operation Manual*, Siemens Industry Inc, Munich, Germany, 2019.
- [29] A. Arif, Z. Wang, J. Wang, B. Mather, H. Bashualdo, and D. Zhao, "Load modeling—A review," *IEEE Trans. Smart Grid*, vol. 9, no. 6, pp. 5986–5999, Nov. 2018.
- [30] A. Alshareef, R. Shah, and N. Mithulananthan, "Influence of motor load on stability of power system with high penetration of large-scale PV," in *Proc. IEEE Ind. Appl. Annu. Meeting*, Detroit, MI, USA, Sep. 2020, pp. 1–5.
- [31] Western Electricity Coordinating Council Modeling and Validation Working Group, "WECC PV power plant dynamic modeling guide," Tech. Rep., 2014.
- [32] S. Stankovic, T. V. Cutsem, and L. Soder, "Fault-current injection strategies of inverters-based generation for fast voltage recovery," *IEEE Trans. Power Syst.*, vol. 37, no. 2, pp. 1543–1553, Aug. 2022.
- [33] K. Kawabe, Y. Ota, A. Yokoyama, and K. Tanaka, "Novel dynamic voltage support capability of photovoltaic systems for improvement of short-term voltage stability in power systems," *IEEE Trans. Power Syst.*, vol. 32, no. 3, pp. 1796–1804, May 2017.
- [34] Y. Xu and F. Li, "Adaptive PI control of STATCOM for voltage regulation," *IEEE Trans. Power Del.*, vol. 29, no. 3, pp. 1002–1011, Jun. 2014.
- [35] P. H. Divshali and L. Söder, "Improving PV dynamic hosting capacity using adaptive controller for STATCOMs," *IEEE Trans. Energy Convers.*, vol. 34, no. 1, pp. 415–425, Mar. 2019.

- [36] A. Boričić, J. Torres, and M. Popov, "Comprehensive review of short-term voltage stability evaluation methods in modern power systems," *Energies*, vol. 14, p. 4076, Jul. 2021.
- [37] J. Liu, C. H. Tan, T. Badrick, and T. P. Loh, "Moving standard deviation and moving sum of outliers as quality tools for monitoring analytical precision," *Clin. Biochem.*, vol. 52, pp. 112–116, 2018.
- [38] F. Neri, *An Introduction to Inner Product Spaces: Euclidean Spaces, Linear Algebra for Computational Sciences and Engineering*. New York, NY, USA: Springer, 2019, pp. 325–338.
- [39] M. T. Nair and A. Singh, *Linear Algebra*. Singapore: Springer, 2018, pp. 163–208.
- [40] Z. Shi, Y. Guan, and X. Li, *Formalization of Complex Analysis and Matrix Theory*. Singapore: Springer, 2020, pp. 135–150.
- [41] A. Mohammad-Djafari, "Entropy, information theory, information geometry and Bayesian inference in data signal and image processing and inverse problem," *Entropy*, vol. 17, no. 6, pp. 3989–4027, 2015.
- [42] Y. Liu and V. Vittal, "Distribution side mitigation strategy for fault induced delayed voltage recovery," in *Proc. IEEE PES Gen. Meeting | Conf. Expo.*, Jul. 2014, pp. 1–5.
- [43] T. Lan, H. Sun, Q. Wang, and B. Zhao, "Synthesis load model with renewable energy sources for transient stability studies," *IEEE Trans. Power Syst.*, vol. 39, no. 1, pp. 1647–1663, Jan. 2024.
- [44] B. Sapkota and V. Vittal, "Dynamic VAR planning in a large power system using trajectory sensitivities," *IEEE Trans. Power Syst.*, vol. 25, no. 1, pp. 461–469, Feb. 2010.
- [45] T. Aziz, M. J. Hossain, T. K. Saha, and N. Mithulanathan, "VAR planning with tuning of STATCOM in a DG integrated industrial system," *IEEE Trans. Power Del.*, vol. 28, no. 2, pp. 875–885, Mar. 2013.
- [46] R. F. Mochamad and R. Preece, "Assessment the impact of VSC-HVDC on the interdependence of power system dynamic performance in uncertain mixed AC/DC systems," *IEEE Trans. Power Syst.*, vol. 35, no. 1, pp. 63–74, Jan. 2020.
- [47] M. Wang and J. V. Milanovic, "Simultaneous assessment of multiple aspects of stability of power systems with renewable generation," *IEEE Trans. Power Syst.*, vol. 39, no. 1, pp. 97–106, Jan. 2024.



ABDULRHMAN ALSHAREEF (Member, IEEE) received the B.Sc. and M.Eng. degrees in electrical engineering from King Abdulaziz University, Jeddah, Saudi Arabia, in 2009 and 2014, respectively, and the Ph.D. degree from The University of Queensland, in 2023. In 2017, he joined the Electrical and Electronic Engineering Department, University of Jeddah, as a Lecturer. He was a Planning Engineer at the EHV Planning Department, Saudi Electricity Company (SEC). He attended

numerous short courses and on-the-job training with manufacturers and consultants worldwide, such as ABB, Hyundai, SNC LAVALIN, and Mott Macdonald Ltd. He delivered several PSS[®]E training sessions for SEC engineers. His current research interests include power system stability, large-scale PV integration impact, delayed voltage recovery issues, power system planning and operation, and analytical studies.



RAKIBUZZAMAN SHAH (Senior Member, IEEE) received the M.Eng. degree from the Asian Institute of Technology, Bangkok, Thailand, and the Ph.D. degree from The University of Queensland, Australia. He is currently an Associate Professor in smart power systems engineering with Federation University Australia (FedUni Australia). Before joining FedUni Australia, he had worked with the University of Manchester, The University of Queensland, and Central

Queensland University. He has experience working at, and consulting with, DNOs and TSOs on individual projects and collaborative work on a large number of projects, primarily on the dynamic impact of integrating new

technologies and power electronics into large systems. He has more than 120 international publications (journals and conferences) and has spoken at the leading power system conferences around the world. His research interests include future power grids, such as renewable energy integration and wide-area control, asynchronous grid connection through VSC-HVdc, power system stability and dynamics, application of data mining in power systems, application of control theory in power systems, distribution system energy management, and low carbon energy systems. He has lead industry projects worth \$3.82 million in the last four years in the area of his research interest.



N. MITHULANATHAN (Senior Member, IEEE) received the B.Sc. (Eng.) degree from the University of Peradeniya, Sri Lanka, the M.Eng. degree from the Asian Institute of Technology (AIT), Bangkok, and the Ph.D. degree from the University of Waterloo, Canada. Prior to joining The University of Queensland, he was attached to the energy field of study at AIT. His previous professional positions include a Planning Engineer at the Generation Planning Division for two years at Ceylon

Electricity Board, Sri Lanka, and the Project Leader with the Centre of Excellence in Electric Power Technology, Chulalongkorn University, Thailand, for one year. Since July 2019, he has been the Director of the Higher Degree Research Training and a Post Graduate Coordinator with the School of Information Technology and Electrical Engineering, The University of Queensland. His main research interests include analytical studies on electric power grids, power system stability and dynamics, grid integration of renewable energy, battery energy storage, and electric vehicle charging stations.



UMER AKRAM (Member, IEEE) received the B.Sc. degree (Hons.) in electrical engineering from the COMSATS Institute of Information Technology, Abbottabad, Pakistan, in 2013, the M.Sc. degree in electrical engineering from the King Fahd University of Petroleum and Minerals, Saudi Arabia, in 2018, and the Ph.D. degree in electrical engineering from The University of Queensland, Australia. His current research interests include modeling, monitoring, and control of

modern power systems and grid-level energy storage systems.



SAEED ALZHRANI (Member, IEEE) received the B.Sc. degree in engineering from the King Fahd University of Petroleum and Minerals (KFUPM), Saudi Arabia, in 2009, the M.Eng. degree from The University of Queensland, Australia, in 2015, and the Ph.D. degree from the Power, Energy and Control Engineering Research Group, School of Information Technology and Electrical Engineering, The University of Queensland, Brisbane, Australia, in 2022. His main

research interests include large-scale renewable energy integration and power system stability studies.

...